This article has been accepted for publication in IEEE Open Journal of Antennas and Propagation. This is the author's version which has not been fully edited and content may change prior to final publication. Citation information: DOI 10.1109/OJAP.2024.3358373

IEEE Open Journal of Antennas and Propagation

Connected Antenna Arrays with Beamsteering Capability for On-Package Millimetre-Wave Applications

MD RASHEDUZZAMAN AL-AMIN[1], STUDENT MEMBER, IEEE, REZA SHAMSAEE MALFAJANI[1], GRADUATE STUDENT MEMBER, IEEE, ELHAM BALADI[1], MEMBER, IEEE, AND MOHAMMAD S. SHARAWI[2], FELLOW, IEEE

[1]Department of Electrical Engineering, Poly-Grames Research Center, Polytechnique Montréal, Montréal, QC, H3T 1J4 Canada
[2]Blue Origin LLC, Kent, WA, 98032 USA

CORRESPONDING AUTHOR: MD RASHEDUZZAMAN AL-AMIN(e-mail: md-rasheduzzaman.al-amin@polymtl.ca).

ABSTRACT In this work, on-package, beamsteerable, slot-based connected antenna arrays (CAA), namely a single slot connected antenna array (SSCAA) and a double slot connected antenna array (DSCAA), are designed, fabricated and measured for millimeter-wave (mm-wave) applications. Both structures are designed in a multi-layer stack-up fashion considering the package environment. The proposed SSCAA and DSCAA show 12.3% (centered at 27.55 GHz) and 16.5% (centered at 30.2 GHz) of measured bandwidths (-10 dB return loss) in their respective operating frequency bands. The measured realized gains of the SSCAA and DSCAA are 9.89 dBi and 12.5 dBi at broadside, demonstrating efficiencies of 89% and 78% respectively. The measured beamsteering capabilities show that the beam from both structures can be steered up to $\pm 35^0$. The proposed SSCAA and DSCAA prototypes are designed having radiator sizes of (1.63λ x 0.17λ x 0.1λ) and (1.61λ x 0.48λ x 0.1λ) respectively (λ centered at 28 GHz). The comparative analysis with the state of the art demonstrates that the proposed SSCAA and DSCAA have excellent bandwidth, high realized gain, and comparable beamsteering performance while presenting a smaller form factor making them suitable for handheld and mobile terminals.

INDEX TERMS Antenna on-package, Beamsteering, Connected Slot Antenna Array, Millimeter-Waves.

I. INTRODUCTION

FIFTH generation (5G) and beyond 5G of wireless communication networks are to provide higher data rates, lower latency, and massive device connectivity. To facilitate such characteristics, antenna systems are required to provide wider bandwidth, higher gain, and steerable beam patterns. In this context, one important enabling technology is the utilization of mm-wave frequency bands for 5G [1]–[3] with the intent of having a wide transmission bandwidth. However, the wireless communication link at the mm-wave spectrum has higher path loss due to the attenuation by the rain and atmospheric absorption. For these causes, antennas with higher gain are required to combat the additional path loss and to relax the requirements on the power amplifiers. Different types of antenna systems are proposed to meet the requirements of the 5G system, but they suffer from different issues including complexity in implementations, larger form factors, limited bandwidth, gains, and radiation patterns [3]–[5].

Antenna in package (AiP) is an important mainstream technology for wireless technologies developed for 5G and beyond. AiP is a viable technique that has become popular recently, for integrating the circuit components and devices with the antennas following various packaging technologies [2], [4]–[6]. The radio die is arranged along with the antenna elements stacking up in multiple layers. After that, the radio frequency integrated circuit (RFIC) is placed at the lower side of the package using the wire bonding connection or the flip-chip technique. Since the dimensions of an antenna are related to its operating frequency and the wavelength in the mm-wave regime is very small, the physical dimensions of the antenna are reduced and become comparable to the dimensions of integrated circuit (IC) packages. This facilitates the integration of the antenna array with other active mm-wave circuits and components. Hence the concepts of the antenna on chip (AOC) and antenna in package (AiP) have come into existence. AiP makes it possible to decrease the transmission losses in the interconnects and the transmission lines between the antennas and the radio dies. It is seen that on/in-package antenna arrays are expected to provide the required performance for the mm-wave communication systems owing to their small form factor, reduced cost, compactness, and reproducibility [5]–[7].

This work is licensed under a Creative Commons Attribution 4.0 License. For more information, see https://creativecommons.org/licenses/by/4.0/

This work is licensed under a Creative Commons Attribution-NonCommercial-NoDerivatives 4.0 License. For more information, see https://creativecommons.org/licenses/by-nc-nd/4.0/

This article has been accepted for publication in IEEE Open Journal of Antennas and Propagation. This is the author's version which has not been fully edited and content may change prior to final publication. Citation information: DOI 10.1109/OJAP.2024.3358373

It can be seen in the literature that various mm-wave frequency bands are considered and explored for probable antenna deployment for 5G wireless communication systems. The selected frequencies of operation vary in accordance with combating high propagation losses in addition to effects such as blockage and multi-path fading. Different types of packaging technologies such as low-temperature co-fired ceramic (LTCC), multi-layer printed circuit board (PCB), multi-layer organic (MLO) substrates, glass substrates, silicon substrates, ball grid array (BGA), liquid crystal polymer, high-density interconnect (HDI) and flip-chip chip-scale package (FcCSP) are currently being implemented [2]–[4], [6], [8], [9]. These packaging technologies are considered for designing mm-wave antennas and for integration with mm-wave circuits.

The available space in handheld devices is limited. Thus, only a small number of sub-arrays can be accommodated within the restricted space. The sub-arrays are placed at the edges of the phone along with their connection to the RFIC and the beamforming module. Moreover, the feeding techniques in the integrated scenario for various antenna array placements are different and complex in nature [8]–[10].

Various types of antenna elements and antenna arrays are utilized for covering the mm-wave spectrum. Patch, dipole, slot, Yagi-Uda, DRA and grid array are considered by researchers [2]–[8]. The majority of the previous works have used patch antenna elements on the package of integrated circuits. Such patch-based arrays have narrow bandwidths and cannot easily cover multi-band. In [9], a miniaturized AiP having multi-band operation and dual polarization for 5G mm-wave technologies is presented. Band switching has been utilized among the ports for covering the two bands. The AiP has five metal layers and has a bandwidth from 27.21 GHz to 28.72 GHz and from 36.96 GHz to 40.17 GHz. The peak realized gain for both polarizations are 10.06 dBi at 28.0 GHz and 10.63 dBi at 39.0 GHz. The overall dimensions of the AiP array are 0.84 mm × 4.20 mm × 19.20 mm (0.068λ x 0.34λ x 1.55λ at 24.25 GHz). Another AiP design was fabricated based on an unbalanced substrate incorporating four metal layers having thick cores at 28 GHz [10]. The presented stack-up provides resistance to the warpage and improves the radiation conditions. The AiP consists of a 1x4 patch array having a bandwidth of 4.3 GHz with a gain of 10.8 dBi. No beamforming capabilities were shown for the designed AiP in the aforementioned work. The dimensions of the designed AiP were 30 mm x 16 mm x 992 µm.

Qualcomm has also proposed mm-wave antenna array modules with that are to be placed on the edges of the cellphones. For covering all radiation directions, it has been proposed that two AiPs be placed on the front top corners, one AiP in the front middle edge and one AiP on the back bottom corner of the cellular phone. A 4x2 patch array was implemented on the left side, a 4x1 dipole array on the right side, and another two 2x1 dipole arrays on the top and bottom sides of the AiP. With these four arrays, spatial and polarization diversities along with dual polarization operations were realized [4], [7], [11]–[16]. In [17], a co-planar fed 1x4 patch antenna array is proposed for mm-wave applications covering the 5G NR bands 23-30.5 GHz. The array has four sets of 2x3 parasitic square arrays for improving both the impedance matching and isolation. The proposed array has a maximum gain of 9.76 dBi, and a total efficiency greater than 68%. The array has overall dimensions of 26 × 5 × 1.524 cubic mm while it can steer the beam up to ±40° in simulation and up to ±30° in measurements at 27 GHz. Miniaturized AiP for mm-wave smartphone is presented in [18] for both broadside and endfire array operation consisting of patch and dipole arrays respectively. The AiP demonstrates dual band operation at 28 and 39 GHz, having a 3GHz bandwidth and a 11.6 dBi gain for broadside and 10 dBi gain for endfire operation. The proposed antenna has dimensions of 5.8 mm × 19 mm × 1.122 mm. Multi- layer reactive impedance surface is used for miniaturizing the patch antenna. Tightly coupled T-shape side via wall and vertically bent folded dipoles were implemented for improving the bandwidth and miniaturizing the antenna for the endfire array. In [19], a 4x4 patch array based AiP is proposed for 5G mm-wave applications, which has high isolation and can be manufactured using low cost PCB technology. High isolation was achieved in the four layer metal stack-up AiP using defected ground structures, capacitive probes, and rotated-fed method. The proposed AiP has a bandwidth of 3GHz (26.5-29.5 GHz) and a peak gain of 17.37 dBi at 28 GHz having the dimension of 37.2 mm x 37.2 mm x 1.2 mm. The AiP can steer the beam up to ±30° in measurements for both E- and H-planes.

A slot-based CAA having 4-elements was engraved in the metal rim of the mobile terminal for mm-wave bands in [20]. The SCAA was reported to have more than 6 GHz of bandwidth and an average realized gain of 8.2 dBi in the mm-wave regime. The SCAA was shown to steer the beam between ±30° from the broadside direction. In addition to that, dual band operation was reported by sharing the same aperture for both microwave and mm-wave bands. The multi-band CAA provided a bandwidth of 3.5 GHz and a realized gain of 8 dBi on average over the mm-wave bands while the CAA demonstrated 140 MHz of bandwidth and 2.5 dBi of measured gain in the microwave band.

Maintaining antenna performance in terms of the radiation pattern for beamforming and beam-scanning, high gains, and wider bandwidth is crucial for mm-wave communication systems. In addition to that, reduced cost with good thermal stability are other important requirements for the on/in package antenna systems. All these together present tremendous technological challenges [2]–[4], [7], [8]. In this paper, the focus has been made on designing the antenna system based on CAA for the on-package environment for next-generation wireless communication systems. Connected antenna arrays

This work is licensed under a Creative Commons Attribution-NonCommercial-NoDerivatives 4.0 License. For more information, see https://creativecommons.org/licenses/by-nc-nd/4.0/

This article has been accepted for publication in IEEE Open Journal of Antennas and Propagation. This is the author's version which has not been fully edited and content may change prior to final publication. Citation information: DOI 10.1109/OJAP.2024.3358373

(CAA) are expected to provide wider bandwidths, lower cross-polarization levels, and required radiation pattern with beam-scanning properties but in a smaller form factor in the on/in-package scenario. In this pursuit, a SSCAA and a DSCAA are designed and analyzed at 28 GHz for overcoming the limitations of antenna modules such as smaller bandwidth, large form factors, and narrower scanning angles. The two proposed solutions have smaller form factors as compared to other antenna modules shown in the literature, which will allow far more integration of other circuits and devices including higher density of antenna elements.

The remainder of the paper is organized as follows: the detailed design of the SSCAA and the DSCAA are presented in Section II. The qualitative analysis for both the SSCAA and the DSCAA are carried out in Section III. The in-house fabricated beamformer is presented in Section III as well for steering the beam. Comparative analysis of the presented work with the state of the art is covered towards the end of the Section III. A comprehensive conclusion is drawn in Section IV.

II. MODELLING OF MM-WAVE CAA

CAAs are array of two or more antenna elements that are electrically connected. The mutual coupling between the elements provides constant current distribution, which results in wider bandwidth. CAAs provide better polarization purity and wide scanning angles [21]–[23]. Slot-based CAA (SCAA) is used in this work to design the proposed AiP for mm-wave mobile terminal applications. The designed AiP can be placed on the edges of the mobile phones as shown schematically in Fig. 1. The antenna module is shown in one edge of the handheld device. The magnified view of the designed antenna is shown in Fig.1 (b). A long slot is made on the ground plane, which is excited with four feeders (dashed lines).The multi-layer stack-up containing the different layers is shown in Fig.1 (c) which includes the feed lines, the BR, branched-out feed lines at the bottom layer, and three different dielectric layers.

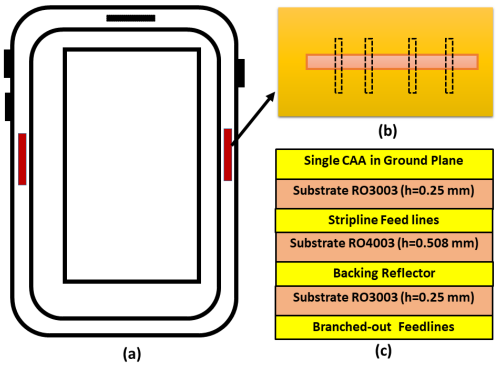


FIGURE 1. : (a) Representative diagram of the on-package CAA placed on one of the edges of the mobile terminal, (b) magnified view of the SSCAA, and (c) layer stack-up of the SSCAA.

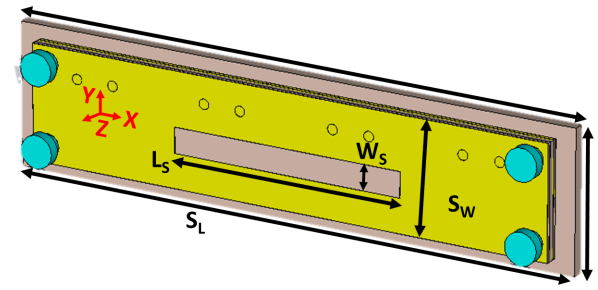
A. SINGLE SLOT CAA

A single SCAA is designed in CST microwave studio to operate at 28 GHz in the mm-wave regime. The front and back view of the on-package SSCAA are presented in Fig. 2(a) and 2(b), respectively. A long slot (17.5 mm x 1.9 mm) is cut in the centre of the topmost ground plane. RO3003 ($\epsilon = 3$, $tan\delta = 0.001$) is used as the first substrate in the design. The thickness of the substrate is chosen as $h = 0.25$ mm keeping the packaging structure in mind. The long slot is excited by four feed lines, which are printed on the opposite side of the first substrate, thus forming a linear array consisting of four elements. It was demonstrated in [23] that the BR is to be placed beneath the first substrate with an air layer in between them. The air layer is replaced with a second substrate to give the antenna a rigid and compact form. RO4003 ($\epsilon = 3.55$, $tan\delta = 0.0027$) is utilized as the second substrate with a thickness of $h = 0.508$ mm. The ideal scenario would be placing the BR 0.25λ (2.67 mm) apart, which would make the AiP really bulky. Parameter sweeps for this separation were conducted in [24] where it was optimized to have a separation of 0.78 mm (0.07λ). Another important factor in the choice of the BR separation is the availability of substrate materials having the desired thicknesses. Thus, a RO4003 substrate with a thickness of 0.508 mm is utilized making the BR separation 0.05λ only. This arrangement gives the feed lines a stripline configuration as the feed lines are embedded in between two substrates surrounded by two metal (top and bottom) layers. Through vias are employed for passing the signals from the bottommost layer to the striplines layer. These vias are shown in Fig. 2(c). Ground connections of the topmost metal layer are realized using eight through vias as shown in Fig. 2(c). Four mini-SMP connectors (PE44489) are utilized at the bottom side of the SSCAA as shown in Fig. 2(d). Four screws are attached on the four corners for holding the different layers in addition to the adhesive glue (epoxy, $\epsilon = 3.5$, $tan\delta = 0.03$).

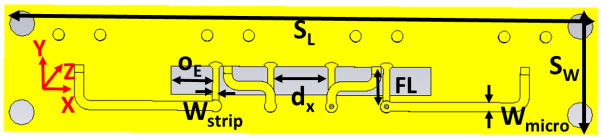
The multi-layer stack-up of the four metal and the four dielectric layers of the SSCAA are depicted in Fig. 3(a). A single slot is cut on the topmost metal layer (M4). The M4 layer is printed on the substrate RO3003 (S4). The feed lines are realized on the metal layer (M3) implemented on the substrate RO4003 (S3). The feed lines have a radial stub at the upper end for better matching and pads at the lower end for connecting to the through vias (TRV) . BR is materialized with metal layer (M2) and implemented on the substrate (S2) for directing the radiation in the broadside direction. This two layers (M2 and S2) have the holes and the antipads for passing the TRV from the lower layers to the upper layers. On the opposite side of the S2, branched feed lines and connector pads (M1) are realized. There are four dielectric layers used in the stack-up of the single slot CAA. The first dielectric layer (RO4003 substrate material (S1) with a thickness of 0.75 mm) is the thickest one, which is used for making the structure rigid enough to hold the

This work is licensed under a Creative Commons Attribution-NonCommercial-NoDerivatives 4.0 License. For more information, see https://creativecommons.org/licenses/by-nc-nd/4.0/

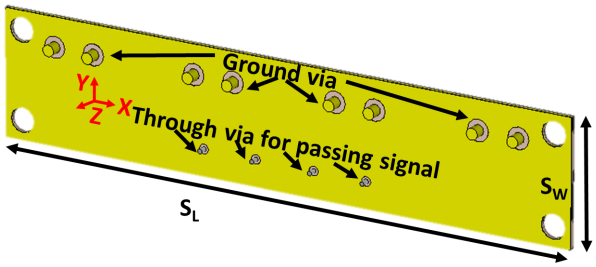
This article has been accepted for publication in IEEE Open Journal of Antennas and Propagation. This is the author's version which has not been fully edited and content may change prior to final publication. Citation information: DOI 10.1109/OJAP.2024.3358373



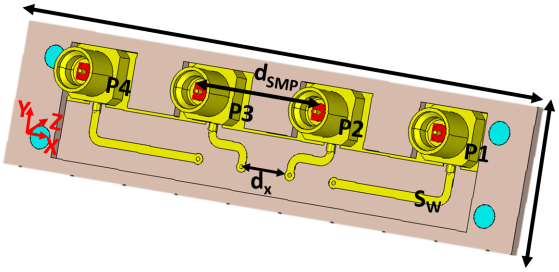
(a)



(b)

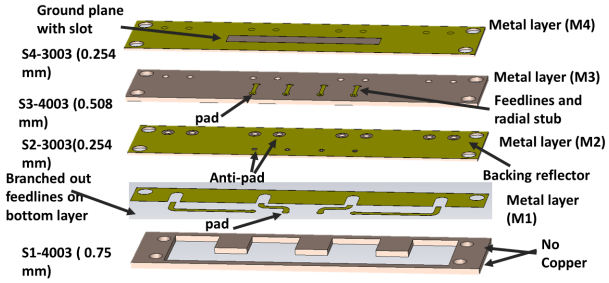


(c)

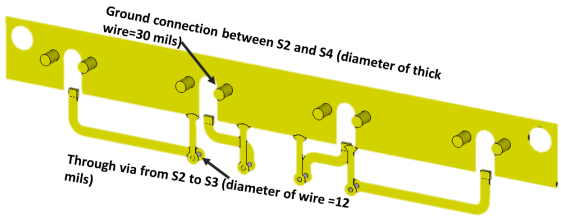


(d)

FIGURE 2. **(a) Front view of the the single SCAA, (b) back view of the single SCAA, (c) through vias for passing the signals from the bottom layer to the striplines and eight ground vias, and (d) mini-SMP connectors and thick substrates for supporting purposes.**



(a)



(b)

FIGURE 3. **(a) Multi-layer stack-up containing various layers of the SSCAA, (b) through vias for ground connections and signal transmission from layer M1 to M3.**

connectors and the stress of the cables. The second substrate (S2) layer is used for housing the BR for directional gain on one side. The branched-out feedlines are designed on the other side of this substrate layer. The third substrate (S3) layer essentially provides the separation between the CAA and the BR, which tremendously affects the bandwidth. The fourth substrate (S4) layer houses the CAA on the upper side whereas the feed lines are printed on the bottom side. The thickness of each substrate is important as it affects the matching significantly. The branched out feed lines are designed using the microstrip technology. Although co-planar waveguide (CPW) lines are also a good fit for mm-wave applications, microstrip lines are chosen due to the limited space availability. The width of the substrate is taken as 7.8 mm in the Y direction owing to the fact that the width of the smartphones are in this range. The dimension of the mini-smp connector in the Y direction is 4.2 mm, which does not leave enough room for implementing GCPW in SSCAA. However, in the design of DSCAA, CPW-based branched out feed lines are implemented. TRVs are utilized for two purposes in the design as depicted in Fig.3(b); firstly, eight TRVs are employed from layer M1 to M4 for realizing the ground in the topmost plane and secondly, four TRVs are designed from layer M1 to M3 to pass the signals from the connectors to the feed lines for exciting the CAA on layer M4.

This work is licensed under a Creative Commons Attribution-NonCommercial-NoDerivatives 4.0 License. For more information, see https://creativecommons.org/licenses/by-nc-nd/4.0/

This article has been accepted for publication in IEEE Open Journal of Antennas and Propagation. This is the author's version which has not been fully edited and content may change prior to final publication. Citation information: DOI 10.1109/OJAP.2024.3358373

A comprehensive parametric analysis was carried out for finding out the optimum dimensions of this SSCAA. The effect of different geometrical parameters including the length of the slot L_S, width of the slot W_S, inter-element spacing d_x, offset from the edge O_E, feed-line length F_L, radius of the radial stub rad were studied using full-wave simulations in CST. There are four ports in the symmetric linear array wherein port 1 and port 4, and port 2 and port 3 resemble one another closely. As such, only results of the parametric study for port 1 and port 2 are provided in Fig. 4. The key observations from the analysis are that the length and the width of the slots determine the resonant frequency. The width of the feed-line plays an important role in obtaining 50 ohm matching whereas the length of the feed-line helps in both wider bandwidth operation and in achieving constructive interference of the fields for optimum gain from the antenna. CAAs are the types of arrays that are fed at a distance between $\lambda/4$ and $\lambda/2$. In the present design, the CAAs are fed at a separation of 0.37λ. In slot antennas, the feeder is usually placed at a $\lambda/20$ offset from the edge for better matching. But the placement of the BR affects the CAA behavior tremendously [22], [23]. In the present on-package design, the BR is placed even closer than the $\lambda/4$ (a round trip of $\lambda/2$ causes constructive interference). For this reason, the parametric sweep of offset from the edge, O_E, was very delicate. A value of 0.3λ is chosen for best performance. The inter-element spacing helps in widening the bandwidth and the constructive interference of the fields for obtaining higher gain. In a similar fashion, the best combination of the parameters were selected for the on-package SSCAA observing the effects of the respective parameters in terms of resonance, matching, and bandwidth. The associated optimum dimensions of the SSCAA are presented in Table 1. The dimensions of the substrates are chosen such that they can accommodate the four mini-SMP connectors and sufficient space is reserved for the cables, adapters etc.

TABLE 1. Geometrical parameters of On-Package SSCAA.

Parameter	Values (mm)	Parameter	Values (mm)
Length of substrate S_L	38	Width of the substrate, S_W	7.8
Length of the slot, L_S	17.5	Width of the slot, W_S	1.9
Spacing in X direction, d_x	3.7	Feed-line length , F_L	2.7
Offset from the edge, O_E	3	Radial stub radius, rad	0.65
distance between mini-SMP connectors, d_{SMP}	10	width of the stripline, W_{strip}	0.43

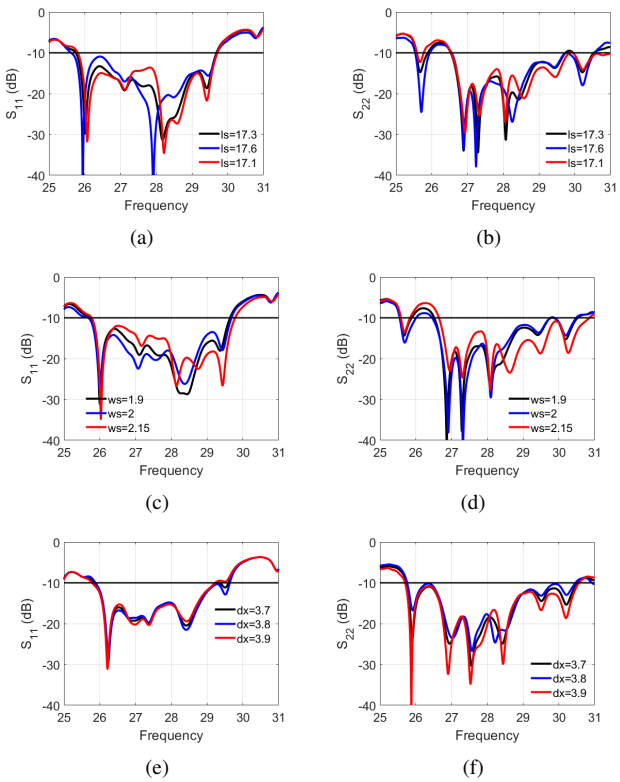


FIGURE 4. Simulated parametric analysis of the on-package SSCAA: (a) effect of the length of the slot L_S on port 1, (b) effect of the length of the slot L_S on port 2, (c) effect of the width of the slot W_S on port 1, (d) effect of the width of the slot W_S on port 2,(e) effect of the inter-element spacing d_x on port 1, and (f) effect of the inter-element spacing d_x on port 2.

B. DOUBLE SLOT CAA

The double slot CAA (DSCAA) is designed for operating at 28 GHz using simulations in CST microwave studio . The front and back view of the on-package DSCAA are presented in Fig. 5(a) and 5(b), respectively. Two long slots (17.3 mm x 1.1 mm) are etched out on the topmost ground plane. The first substrate used in this DSCAA design is RO3003 ($\epsilon = 3$, $tan\delta = 0.001$) having a thickness of $h = 0.25$ mm. The planar slot array (4x2) is excited using four meandered feed lines. The feed lines are printed on the second substrate. RO4003 ($\epsilon = 3.55$, $tan\delta = 0.0027$, $h = 0.508$ mm) is used as the second substratem, below which the BR is placed. The branched-out grounded CPW (GCPW) feed lines are printed on the third substrate, as shown in Fig. 5(b) and 5(d), respectively. On the bottommost layer, four mini-SMP connectors (PE44489) are placed for feeding the planar DSCAA, as shown in Fig. 5(d). The signals from the connectors on the bottommost layer pass to the pads of the four through vias. From this bottommost layer, the signals then pass to the meandered feed lines for exciting the double slots. The through vias are shown in Fig. 5(c). Eight vias are utilized for ensuring the ground connection from the bottommost layer to the topmost layer. The different layers of the structure are glued together with

This work is licensed under a Creative Commons Attribution-NonCommercial-NoDerivatives 4.0 License. For more information, see https://creativecommons.org/licenses/by-nc-nd/4.0/

This article has been accepted for publication in IEEE Open Journal of Antennas and Propagation. This is the author's version which has not been fully edited and content may change prior to final publication. Citation information: DOI 10.1109/OJAP.2024.3358373

adhesive material (epoxy, $\epsilon = 3.5$, $tan\delta = 0.03$). In addition to that, four corner screws are employed for holding them together.

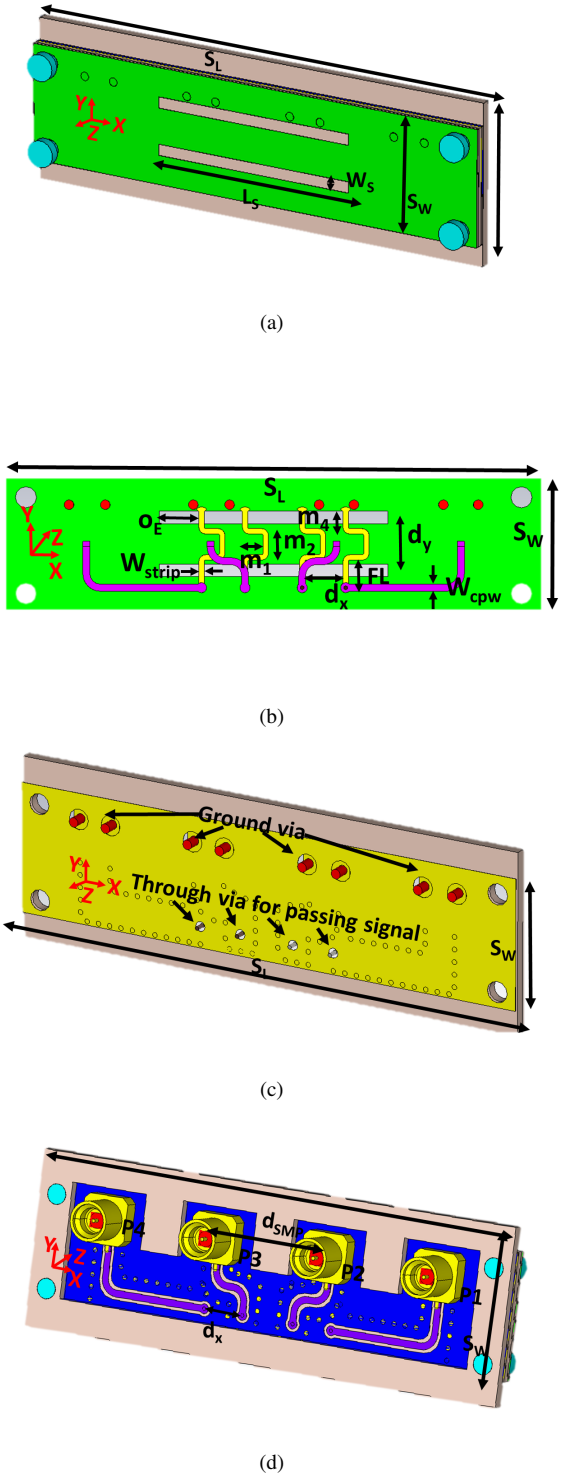


FIGURE 5. (a) Front view of the on-package DSCAA, (b) back view of the the on-package DSCAA, (c) through Vias for passing the signals from the bottom layer to the striplines and ground vias of the on-package DSCAA, and (d) the mini-SMP connectors and thick substrates for supporting purposes.

The multi-layer stack-up of the four metal and three substrate layers of the DSCAA are depicted in Fig. 6(a). Both the simulated and fabricated structures are shown for better comprehension. Two slots are cut on the topmost metal layer (M4). The multi-layer stack-up of the DSCAA follows a similar arrangement as the SSCAA, which was explained in detail in Sec II. A, with some exceptions. The first difference is that the feed lines of layer M3 are longer such that they can excite both the slots. The feed lines are meandered to attain the necessary phase shifts for obtaining the constructive interference of the radiation from both the slots. The two slots are excited with series feeding. The other difference is that the branched out feed lines in layer M1 are realized using the GCPW technology. The GCPW vias are drilled in layer S2.

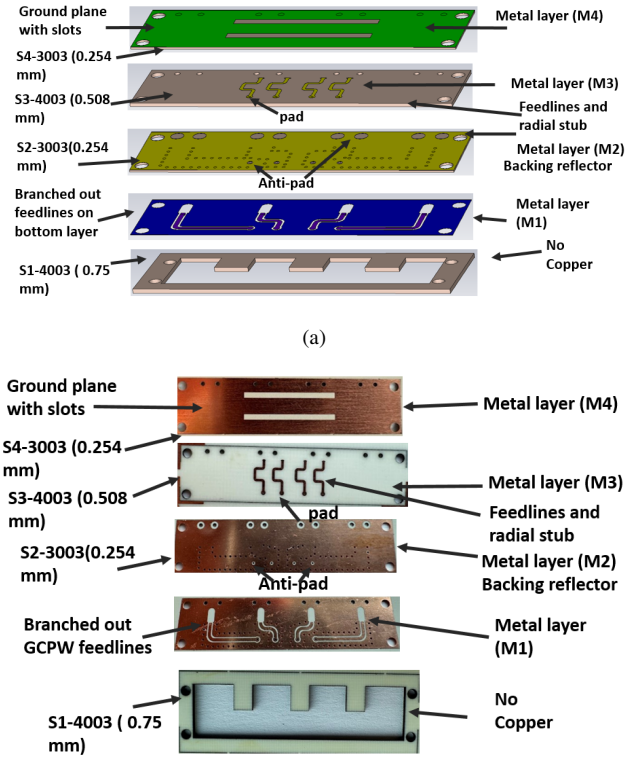


FIGURE 6. (a) Multi-layer stack-up of various simulated layers of on-package DSCAA, (b) multi-layer stack-up of various fabricated layers of on-package DSCAA.

Rigorous parametric analysis is performed in order to find out the best dimensions for the DSCAA. There are various parameters associated with the design of DSCAA, out of which the analysis for the length of the slot L_S, width of the slot W_S, offset from the edge O_E,inter-element spacing in the X-direction d_x, inter-element spacing in the Y-direction d_y, feed-line length F_L, and the radius of the radial stub rad are optimized through full-wave simulations. As discussed in Sec II. A, ports 1 and 4, as well as the ports 2 and 3 are symmetric in nature. Therefore, the S-parameter results of one port from each pair is illustrated

This work is licensed under a Creative Commons Attribution-NonCommercial-NoDerivatives 4.0 License. For more information, see https://creativecommons.org/licenses/by-nc-nd/4.0/

This article has been accepted for publication in IEEE Open Journal of Antennas and Propagation. This is the author's version which has not been fully edited and content may change prior to final publication. Citation information: DOI 10.1109/OJAP.2024.3358373

in Fig. 7 and Fig. 8, respectively. It can be seen that L_S and W_S have a direct effect on the resonance frequency of the DSCAA, whereas the parameters O_E, F_L, and rad have strong influence on the level of matching. Parameters like d_x and d_y have tremendous effect on widening the bandwidth and on the gain enhancement, as known from the array theory. The CAAs are excited at a 0.35λ distance in the X-direction and a 0.41λ distance in the Y-direction. Following these optimizations, the issue of the BR placement and the antipads on the BR layer are addressed for finding the optimum position as the placement of the BR in close proximity disturbs the bandwidth adversely [22], [23]. Tremendous efforts are made for finding the best position of the GCPW vias as well on the bottommost layer. After this comprehensive parametric analysis, best sets of parameters are selected for the final simulation and fabrication of the DSCAA keeping the specifications like resonance, matching, bandwidth, and gain in consideration. The final optimized set of parameters for the on-package DSCAA are presented in Table 2.

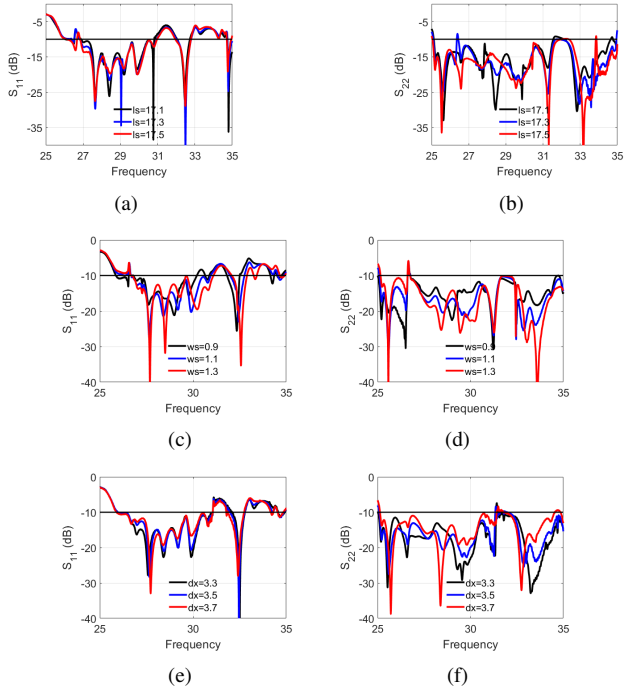


FIGURE 7. Parametric analysis of the on-package DSCAA: (a) effect of the length of the slot L_S on port 1, (b) effect of the length of the slot L_S on port 2, (c) effect of the width of the slot W_S on port 1, (d) effect of the width of the slot W_S on port 2,(e) effect of the inter-element spacing d_x on port 1, and (f) effect of the inter-element spacing d_x on port 2.

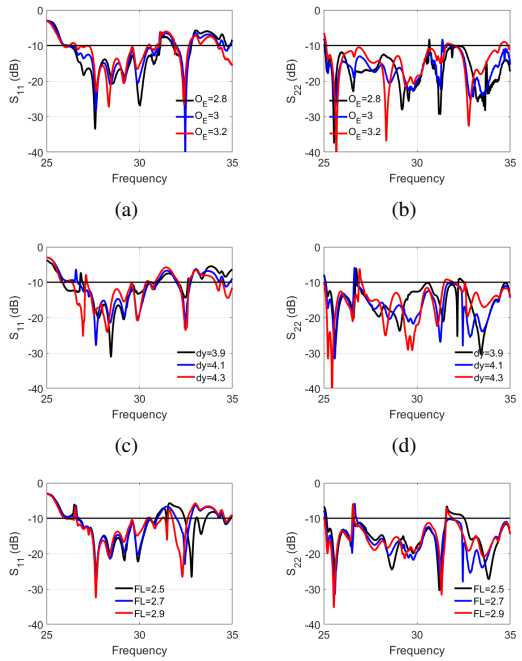


FIGURE 8. Parametric analysis of the on-package DSCAA: (a) effect of the offset from the edge of the slot O_E on port 1, (b) effect of the offset from the edge of the slot O_E on port 2, (c) effect of the inter-element spacing d_y on port 1, and (d) effect of the inter-element spacing d_y on port 2, (e) effect of the feed-line length F_L on port 1, (f) effect of the feed-line length F_L W_S on port 2,

TABLE 2. Geometrical parameters of on-package DSCAA

Parameter	Values (mm)	Parameter	Values (mm)
Length of substrate S_L	38	Width of the substrate, S_W	10
Length of the slot, L_S	17.3	Width of the slot, W_S	1.1
Spacing in the X direction, d_x	3.5	Spacing in the Y direction, d_y	4.1
Offset from the edge,O_E	3	Radial stub radius, rad	0.5
Length of meanderline, m_1	2.1	Length of meanderline, m_2 and m_4	2.2, 1.7

III. RESULTS AND DISCUSSIONS

A. BEAMFORMER DESIGN AND MODELLING

For analyzing the beamsteering performance of the SSCAA, a mm-wave 4-element beamformer is designed using the block diagram depicted in Fig. 9. The path of the signal flow and power controllers are illustrated in Fig. 9. For validating the performance of the various blocks from the beamformer, simulations are carried out in ADS. For the power combiner/divider, (EP2-5G1+) from Mini-circuits is used, which covers the desired frequency range. The high isolation of the power combiner/divider is appropriate for our design. The insertion loss of the (EP2-5G1+) is 1.3 dB, phase imbalance is 1.7^0 , and amplitude imbalance is 0.1 dB. For the phase shifter, a 5-bit digital phase shifter (TGP2100) is utilized that covers the frequency band of 28 GHz to 30 GHz. The insertion loss of the phase shifter is 7 dB. The GCPW transmission line is used and designed in HFSS with RO4003 substrate having a thickness of 8 mil. The width

This work is licensed under a Creative Commons Attribution-NonCommercial-NoDerivatives 4.0 License. For more information, see https://creativecommons.org/licenses/by-nc-nd/4.0/

This article has been accepted for publication in IEEE Open Journal of Antennas and Propagation. This is the author's version which has not been fully edited and content may change prior to final publication. Citation information: DOI 10.1109/OJAP.2024.3358373

of the line is 0.35 mm and the gap is 0.2 mm. The phase shifter is wire bonded using ENIG plating but this plating increases the path loss [25]. A low noise amplifier (LNA) from Analog Devices (HMC1040LP3CE) is used due to the high losses in the beamformer, whose noise figure and gain are 2.2 dB and 22.5 dB, respectively in our frequency band. Although the phase shifter is supposed to cover 348^0, it only covers 330^0 of phase range in practice. Fig. 10 shows the LNA setup, the final prototype of the beamformer, the setup for finding the correct phase from the beamformer, as well as the final fabricated beamformer. The required progressive phase shift is realized by selecting the various combination of the 5-bits of the phase shifter. The phase of the signals are seen on the VNA as shown in Fig. 10 to verify the required phase of the signals.

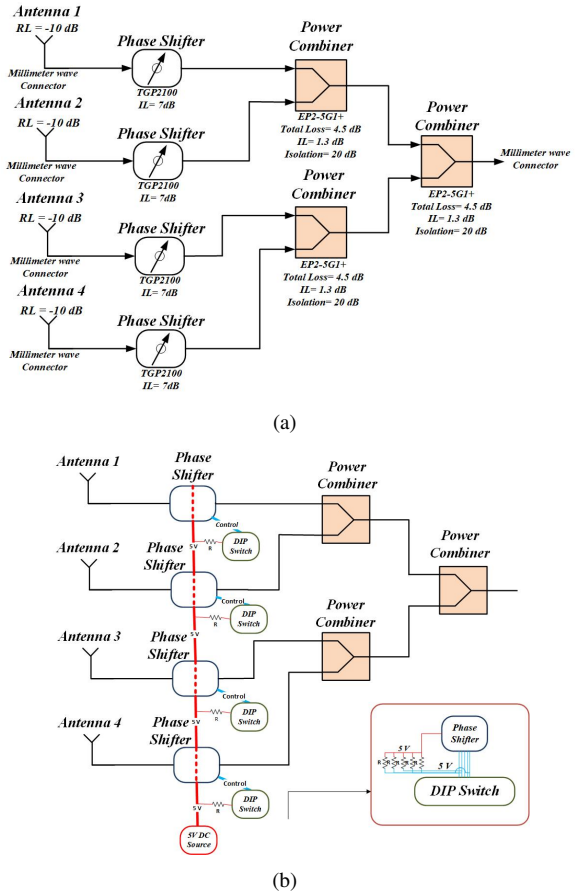


FIGURE 9. Block diagram of the beamformer: (a) signal pass, (b) power flow and controllers.

B. MEASUREMENT RESULTS FOR THE SINGLE SLOT CAA

The front view and back view of the fabricated single SCAA are shown in Fig. 11(a) and Fig. 11(b), respectively. As discussed in Sec II. A, the long slot on the topmost layer, the eight TRVs for ground connections, and the four holes for holding the screws are seen on the back view of the SSCAA. The four microstrip feed lines, four mini-smp connectors,

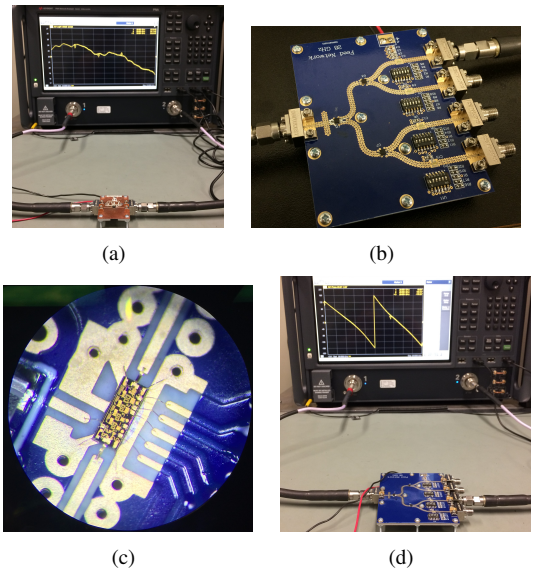


FIGURE 10. Beamformer : (a) LNA setup, (b) the fabricated beamformer, (c) closer view of the wire bonds in the phase shifter, and (d) the beamformer setup for finding out the correct phases.

and the four pads for the signal TRVs are seen on the back view of the SSCAA. The four holes are drilled on the four corners for holding the layers together (in addition to gluing them). A holder is designed for assisting in the measurement stage which is shown in Fig. 11(c).

The S-parameters of the SSCAA is measured by placing the SSCAA on the holder and using the Keysight PNA N5224B covering the frequency range of 25 GHz to 31 GHz. The comparison between the simulated and the measured S-parameters for the four ports are depicted in Fig. 12. The ports 1 and 4 are identical in terms of boundary conditions, and same goes for the ports 2 and 3. The ports 1 and 4 are close to the slot edge at one side and thus they are manipulated due to the edge-born waves [22], [23] while ports 2 and 3 are not affected by such edge effects. Owing to this difference in the boundary conditions, the behavior of ports 1 and 4 is different from ports 2 and 3. The simulated bandwidths for ports 1 and 4 are approximately 3.8 GHz (25.8–29.6 GHz), while the measured bandwidths are at least 5 GHz (25.6–30.6 GHz). For ports 2 and 3, the simulated bandwidth is 4.7 GHz (25.8–30.5GHz), whereas the measured (-9.2 dB) bandwidth is at least 5.13 GHz (25.87–31 GHz). The overall simulated (-10dB return loss) bandwidth for the SSCAA is 3.39 (25.84 GHz–29.23 GHz) and the Overall measured (-10dB return loss) bandwidth is 3.18 GHz (25.87–29.05 GHz). The differences between the simulated and the measured bandwidths are seen because of various fabrication issues such as soldering bumps, whose effects are not negligible in the mm-wave regime. Soldering bumps are not only present in the vicinity of the connectors. Rather, eight ground vias are present, which are connected from the bottom layer to the top layer. The soldering of these TRV pads on the stripline (M2) layer produces solder bumps,

This work is licensed under a Creative Commons Attribution-NonCommercial-NoDerivatives 4.0 License. For more information, see https://creativecommons.org/licenses/by-nc-nd/4.0/

This article has been accepted for publication in IEEE Open Journal of Antennas and Propagation. This is the author's version which has not been fully edited and content may change prior to final publication. Citation information: DOI 10.1109/OJAP.2024.3358373

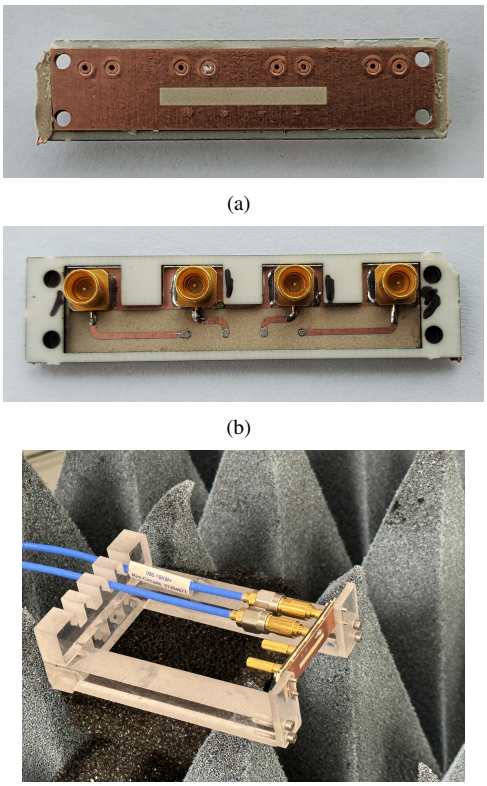


FIGURE 11. (a) Front view of the fabricated SSCAA, (b) back view of the the SSCAA, and (c) the holder for holding the SSCAA during measurements.

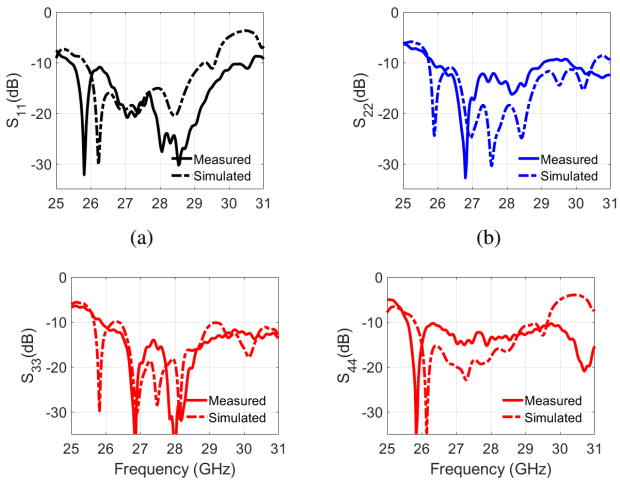


FIGURE 12. Comparison between the simulated and measured S-parameters of the SSCAA, wherein dashed are simulated curves, and solid are measured curves : (a) port 1, (b) port 2, (c) port 3, and (d) port 4.

which result in air gaps in between the layers. In addition to that, four through vias are present for passing the signals to the feed lines. The anti-pads of these four vias, the diameter of the vias and the position of the vias can also significantly affect the bandwidth. The other major difference between the simulation and the fabrication environment is the application of adhesive glue in between the various layers for holding them together, which has affected the behavior of the SSCAA immensely.

The radiation patterns for the four ports of the SSCAA are measured in the quasi far field anechoic chamber at the Poly-GRAMES research center of Polytechnique Montreal. The radiation pattern measurement setup and the close view of the setup for beamsteering are shown in Fig. 13(a) and 13(b), respectively. The normalized radiation patterns comprising the co- and cross-polarization levels for all the four ports are measured from 26.5–30.5 GHz. The comparative plots between the simulation and measurement results of the normalized co- and cross-pol levels at 26.5 GHz, 28 GHz and 29.5 GHz are shown in Fig. 14, Fig. 15, and Fig. 16 respectively. It can be seen that the simulated and measured patterns resemble each other greatly other than some minor discrepancies, which might have arisen from the measurement setup inaccuracies. The measurement setup includes the feeding mast, metal frame, and cables, which do not exist in the simulation environment and are likely to cause ripples in the radiation patterns. The beams are combined at boresight direction for the 26.5, 28, and 29.5 GHz and compared with the measured patterns in Fig. 17. The simulated sidelobe levels (SLLs) of the radiation patterns are lower than -10 dB for all frequencies. The measured SLLs are well below -10 dB for 28 and 29.5 GHz but elevated for 26.5 GHz. The reason for the elevated SLL for 26.5 GHz are due to the poor matching of ports 1 and 4. The simulated and measured gains of the SSCAA at the boresight direction are plotted as a function of frequency in Fig. 18. It is seen that the realized simulated and measured gains depict good agreement across the wide operating frequency range. The discrepancies between the simulated and measured realized gains are most probably caused by the measurement setup differences from the simulation environment.

Beamforming and beamsteering capabilities of the mobile terminal is one of the important attributes of the 5G wireless communication systems. The beamsteering patterns of the SSCAA for the mobile terminal application are simulated using full-wave simulation tools and also measured in the anechoic chamber. For directing the beam towards various angles, the progressive phase shift of every elements of the SCAA is calculated using the equation β=-$kdsin\theta$ where $k = 2\pi/\lambda$, d is the inter-element spacing, θ is the required direction of the beam, and β is the progressive phase shift [26]. The calculated phase shift is applied in the CST simulation environment and the resulting beams are obtained. For examining the beamsteering capabilities of the SSCAA in the experiments, an in-house developed beamformer is utilized. The required phases are applied through the phase shifter of the beamformer for steering the beam to 0^0, 10^0, 20^0, and 35^0. The setup for characterizing the beamsteering performance in the chamber is shown in Fig. 13(b). The beamsteering capabilities of the SSCAA are illustrated in

This work is licensed under a Creative Commons Attribution-NonCommercial-NoDerivatives 4.0 License. For more information, see https://creativecommons.org/licenses/by-nc-nd/4.0/

This article has been accepted for publication in IEEE Open Journal of Antennas and Propagation. This is the author's version which has not been fully edited and content may change prior to final publication. Citation information: DOI 10.1109/OJAP.2024.3358373

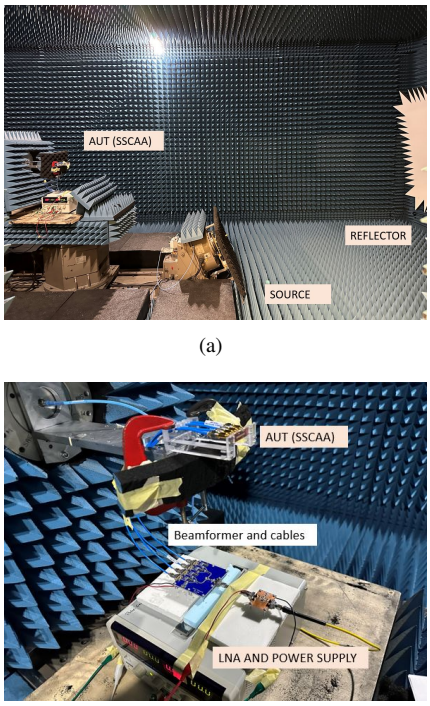


FIGURE 13. **(a) Radiation pattern measurement setup for on-package SSCAA, and (b) the close view of the measurement setup for beamsteering.**

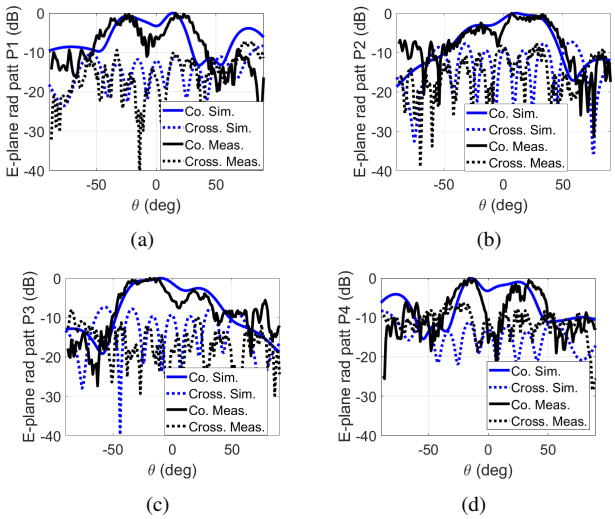


FIGURE 14. **Normalized radiation patterns of the SSCAA comprising both co- and cross-pol levels at 26.5 GHz (a) port 1, (b) port 2, (c) port 3, and (d) port 4.**

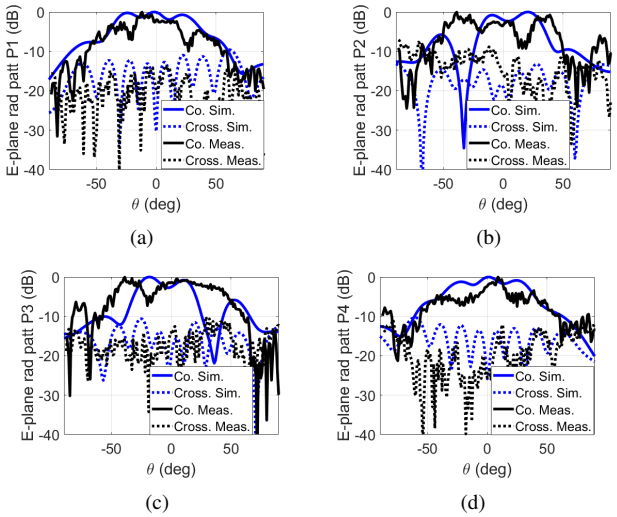


FIGURE 15. **Normalized radiation patterns of the SSCAA comprising both co-pol and cross-pol levels at 28 GHz (a) port 1, (b) port 2, (c) port 3, and (d) port 4.**

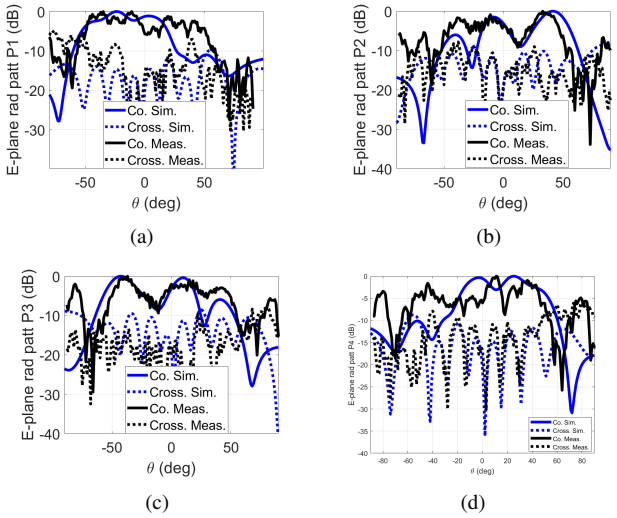


FIGURE 16. **Normalized radiation patterns of the SSCAA comprising both co-pol and cross-pol levels at 29.5 GHz (a) port 1, (b) port 2, (c) port 3, and (d) port 4.**

TABLE 3. **Beamsteering performance of on-package SSCAA**

Beam direction (sim)	Beam direction (meas)	SLL (sim)	SLL (meas)
0^0	0^0	-11.3 dB	-12.5 dB
10^0	9^0	-10.7 dB	-11.2 dB
20^0	21^0	-10.3 dB	-8.39 dB
35^0	35^0	-4.5 dB	-5.3 dB

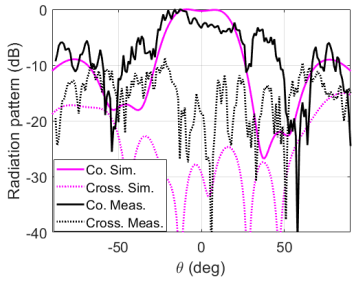
Fig. 19 and tabulated in Table 3. The simulated and measured beams show good agreement. The obtained gain for radiation at 10^0, 20^0, and 35^0 are decreased as the beamsteering angle increases, which is expected. In addition to that, the SLLs are also increased with the increase of the beamsteering angle.

C. MEASUREMENT RESULTS FOR THE DOUBLE SLOT CAA

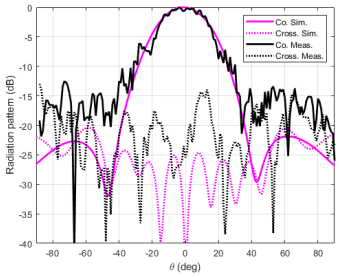
The front and the back views of the fabricated on-package DSCAA prototype are shown in Fig.20(a) and Fig. 20(b), respectively. The stack-up matches what was shown in Fig.

This work is licensed under a Creative Commons Attribution-NonCommercial-NoDerivatives 4.0 License. For more information, see https://creativecommons.org/licenses/by-nc-nd/4.0/

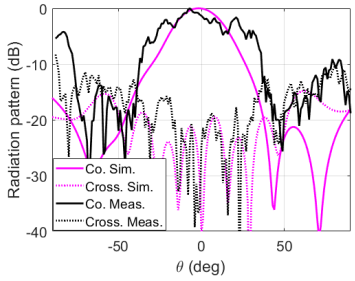
This article has been accepted for publication in IEEE Open Journal of Antennas and Propagation. This is the author's version which has not been fully edited and content may change prior to final publication. Citation information: DOI 10.1109/OJAP.2024.3358373



(a)

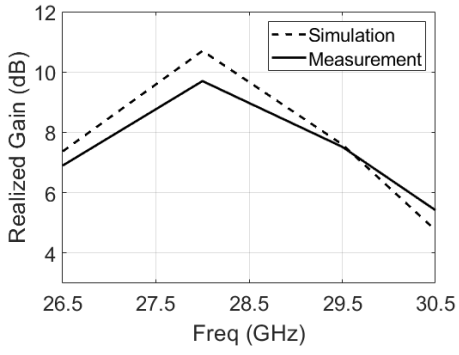


(b)



(c)

FIGURE 17. Normalized combined radiation patterns of the SSCAA comprising both co-pol and cross-pol levels at boresight direction: (a) 26.5 GHz (b) 28 GHz and (c) 29.5 GHz.



(a)

FIGURE 18. Realized gain as a function of frequency at boresight for the SSCAA.

6(b).The different layers are glued with epoxy and assembled tightly with the assistance of four screws at the four corners. The fabricated prototype is fixed using a plastic holder for easier measurement, as shown in Fig. 20.

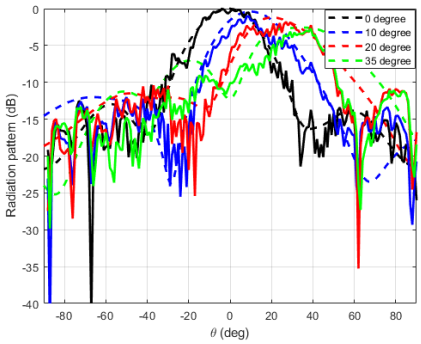
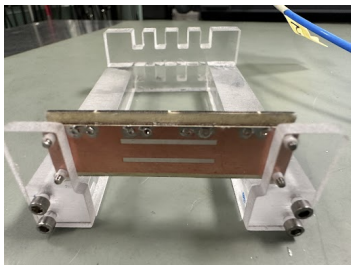


FIGURE 19. Simulated and measured beamsteering response of the SS-CAA; dashed are simulated curves, and solid are measured curves.



(a)



(b)

FIGURE 20. (a) Front view of the fabricated on-package DSCAA, and (b) back view of the fabricated on-package DSCAA.

The S-parameters of the on-package DSCAA are measured using Keysight PNA N5224B over the frequency range of 25 GHz to 35 GHz. The DSCAA is placed on the plastic holder during the measurements. The measured and simulated S-parameters are depicted in Fig. 21. A closer look at the DSCAA reveals that ports 1 and 4 are at the edge of the double slots and ports 2 and 3 are in the middle of the slots. Hence, each pair of ports is expected to show identical behavior. However, the S-parameters of these two pairs of ports are quite different from one another as ports 1 and 4 are at the edge of the slots and therefore greatly influenced by the edge-born waves [21], [22]. The simulated bandwidth of the ports 1 and 4 is 5 GHz (26.1–31.1 GHz). The measured bandwidth of this pair of ports is 5.1 GHz (27.65–

This work is licensed under a Creative Commons Attribution-NonCommercial-NoDerivatives 4.0 License. For more information, see https://creativecommons.org/licenses/by-nc-nd/4.0/

This article has been accepted for publication in IEEE Open Journal of Antennas and Propagation. This is the author's version which has not been fully edited and content may change prior to final publication. Citation information: DOI 10.1109/OJAP.2024.3358373

32.75 GHz). On the other hand, the simulated bandwidth of ports 2 and 3 is 6.52 GHz (25.08–31.6 GHz), while the measured bandwidth is at least 7.15 GHz (27.85–35 GHz). The comparative plots of the S-parameters in Fig. 21 show good agreement between the simulated and measured data over frequency. The overall simulated (-10dB return loss) bandwidth for the DSCAA is 4.93 GHz (26.11 GHz–31.04GHz) and the Overall measured (-10dB return loss) bandwidth is 5 GHz (27.7 –32.7 GHz). It has been reported that the bandwidth of the CAA improves when the CAA is periodic in two dimensions (planar array) compared to the 1D CAA (linear array) [20]. This is evidently observable in the case of the DSCAA. The isolation between the ports is an important parameter to be studied and analyzed. The port isolation between ports 1 and 2, as well as ports 3 and 4, are presented in Fig. 22. The comparative plot between the simulated and the measured port isolation shows that the isolation is lower than -10 dB over the desired bands. Although the ports are well isolated, it is observed that the measured port isolation is lower than the simulated one. The discrepancies between the measured and simulated results are seen because of the difference between the two environments. Firstly, the adhesive glue that is used in between different layers is not present in the simulation environment. The solder bumps of the pads in the feed-line layer have created some unwanted gaps between the layers, which is a potential cause of the difference. Other undesired effects of the fabrication and measurement environments also affect the measured bandwidth. All such differences have caused disagreement between the simulated and measured results.

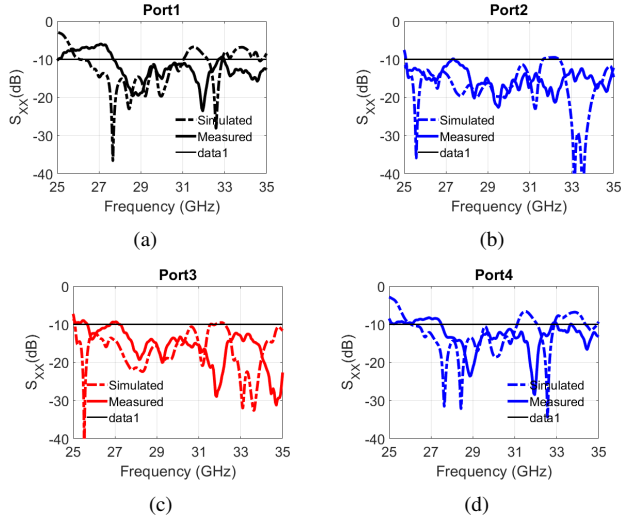


FIGURE 21. Comparison between the simulated and measured S-parameters of the DSCAA, dashed are simulated curves, and solid are measured curves: (a) port 1, (b) port 2, (c) port 3, and (d) port 4.

After measuring the S-parameters, the radiation patterns of the on-package DSCAA are recorded in the anechoic chamber. The setup that is used for the radiation pattern

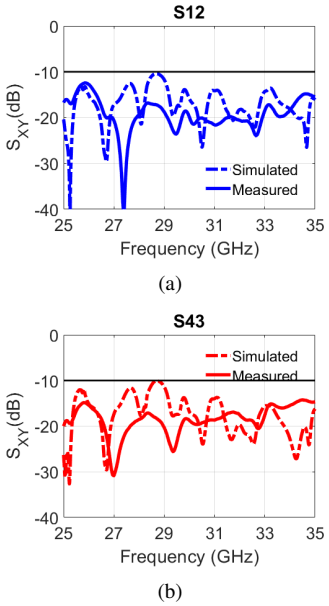


FIGURE 22. Comparison between the simulated and measured port isolation of the DSCAA, dashed are simulated curves, and solid are measured curves: (a) port 1 and port 2, (b) port 3 and port 4.

measurement as well as the setup for tuning the phases of the on-package DSCAA are illustrated in Fig. 23(a) and 23(b), respectively. The normalized radiation patterns of the four ports of the on-package DSCAA are measured at 27, 28, and 31 GHz. The co- and cross-pol normalized radiation patterns for these frequencies are shown in Fig. 24, Fig. 25, and Fig. 26, respectively. Very good agreement is present between the simulated and measured radiation patterns for all three different frequencies. The observed differences are present due to formerly discussed differences between the simulated structure and the measured prototype. The measurement setup in the anechoic chamber contains a metal frame, a feeding mast, and cables, which are not present in the simulation scenario. These differences seem to have caused unwanted ripples in the measured radiation patterns. The radiation patterns from the four ports of the DSCAA are combined in the boresight direction and obtained at 27, 28 and 31 GHz, as illustrated in Fig. 27. The combined broadside patterns have excellent resemblance for all the frequencies. The simulated and measured SLLs fall below -10 dB for every frequencies. The realized gain of the DSCAA is plotted in Fig. 28. The comparison between the simulated and measured realized gains over the frequency range of 27-31 GHz confirms an excellent agreement.

Beamsteering characteristics of the DSCAA are also obtained from the simulated and measured data. Although the DSCAA is a planar array, the phase shifts required for beamsteering are calculated using the same equation used for the SSCAA case, due to the series feeding of the array. The required phase shift is calculated for steering the beam to 10^0, 20^0, and 35^0 and applied in the simulation environment. The beamsteering characteristics of the DSCAA are also

This work is licensed under a Creative Commons Attribution-NonCommercial-NoDerivatives 4.0 License. For more information, see https://creativecommons.org/licenses/by-nc-nd/4.0/

This article has been accepted for publication in IEEE Open Journal of Antennas and Propagation. This is the author's version which has not been fully edited and content may change prior to final publication. Citation information: DOI 10.1109/OJAP.2024.3358373

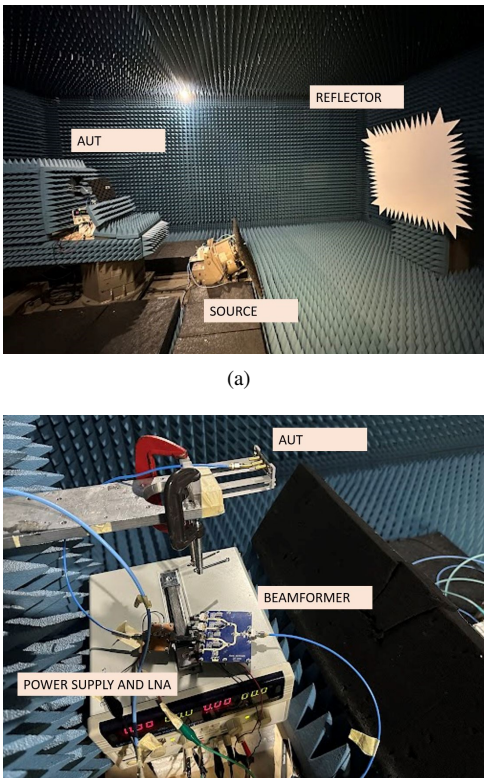


FIGURE 23. **(a) Radiation pattern measurement setup for on-package DSCAA, and (b) measurement setup for tuning the phases.**

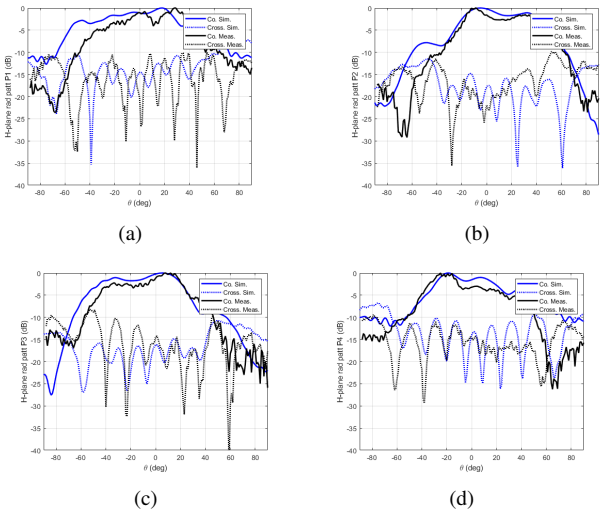


FIGURE 24. **Normalized radiation patterns of the DSCAA comprising both co- and cross-pol levels at 27 GHz for (a) port 1, (b) port 2, (c) port 3, and (d) port 4.**

measured in the anechoic chamber using the in-house built beamformer. The required phase shifts are obtained using the phase shifter of the beamformer. The measured beamsteering characteristics of the on-package DSCAA are depicted in Fig. 29 and tabulated in Table 4. The beams are steered to 10^0, 20^0, and 35^0. It is seen that the gain decreases as the

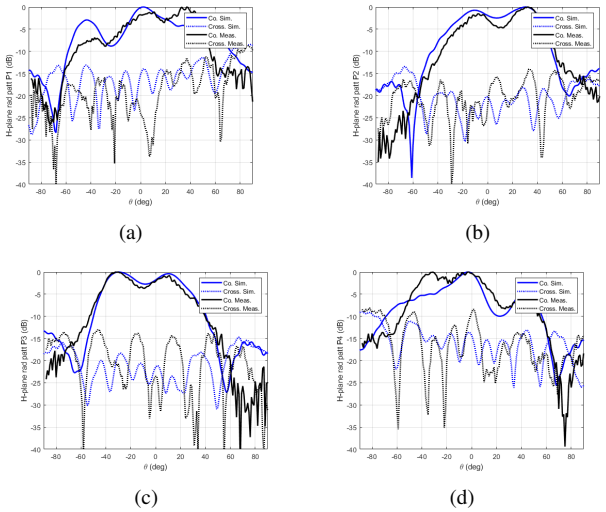


FIGURE 25. **Normalized radiation patterns of the DSCAA comprising both co- and cross-pol levels at 28 GHz for (a) port 1, (b) port 2, (c) port 3, and (d) port 4.**

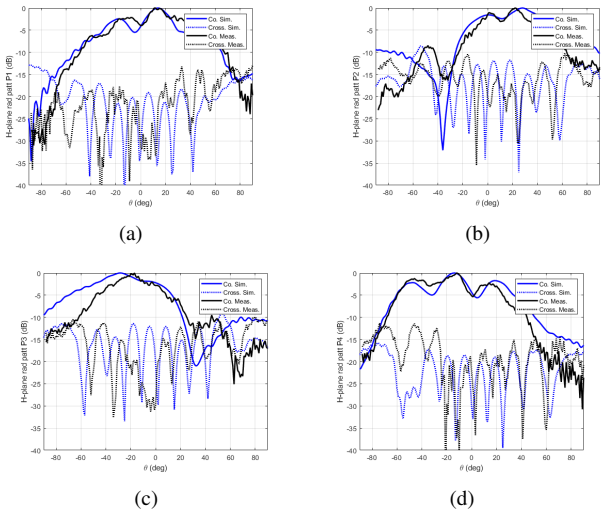


FIGURE 26. **Normalized radiation patterns of the DSCAA comprising both co- and cross-pol levels at 31 GHz for (a) port 1, (b) port 2, (c) port 3, and (d) port 4.**

beamsteering angle is increased. The SLL starts to increase with the increase of the steering angle.

TABLE 4. **Beamsteering performance of on-package DSCAA**

Beam direction (sim)	Beam direction (meas)	SLL (sim)	SLL (meas)
0^0	0^0	-15.5 dB	-14 dB
10^0	8^0	-10.5 dB	-9.45 dB
21^0	21^0	-9.8 dB	-7 dB
35^0	35^0	-7 dB	-9 dB

This work is licensed under a Creative Commons Attribution-NonCommercial-NoDerivatives 4.0 License. For more information, see https://creativecommons.org/licenses/by-nc-nd/4.0/

This article has been accepted for publication in IEEE Open Journal of Antennas and Propagation. This is the author's version which has not been fully edited and content may change prior to final publication. Citation information: DOI 10.1109/OJAP.2024.3358373

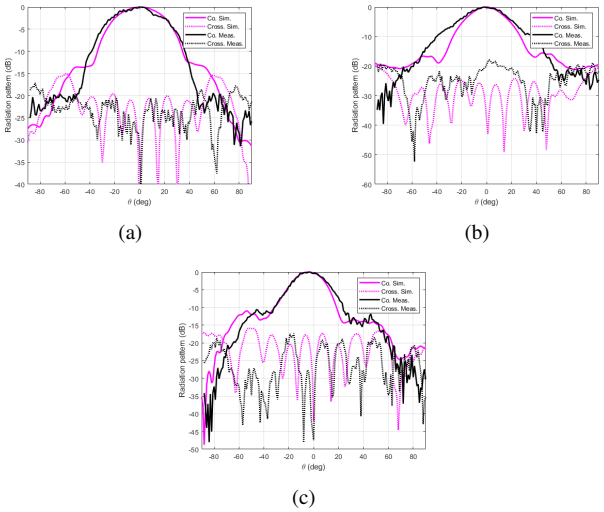


FIGURE 27. **Normalized combined radiation patterns of the DSCAA comprising both co- and cross-pol levels at boresight direction for (a) 27 GHz (b) 28 GHz and (c) 31 GHz.**

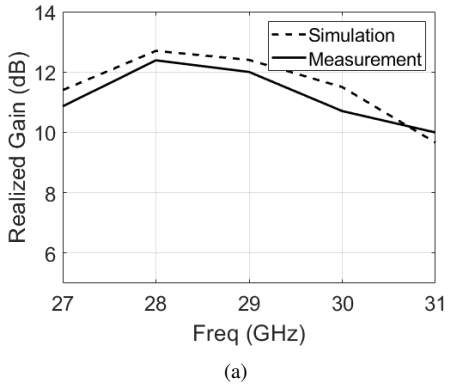


FIGURE 28. **Realized gain as a function of frequency at boresight for the DSCAA.**

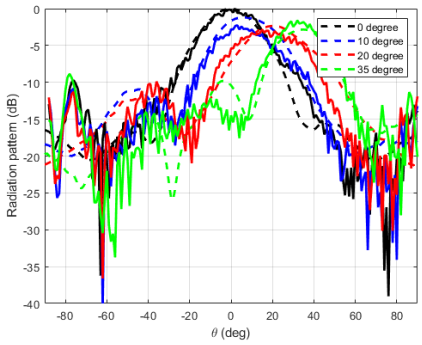


FIGURE 29. **Simulated and measured beamsteering response of the DSCAA; dashed are simulated curves and solid are measured curves.**

D. COMPARISON WITH THE LITERATURE AND CHALLENGES

A comparison table of the on-package SSCAA and DSCAA with the most recent AiPs covering the mm-wave bands of the 5G wireless communication systems is presented in Table 5. The table also covers the comparison of the present work with the available slot-based CAA designs [20], [23]. For example, the proposed SSCAA and DSCAA have wider bandwidths that are at least 4-5 times more than Qualcomm's antenna module while occupying 36% (SSCAA) and 2.2% (DSCAA) lesser areas. The obtained realized gains are comparable with the existing works whereas the beamsteering capabilities of the proposed prototypes are mention worthy. Thus, it is evident from the comparative table that the proposed on-package SSCAA and DSCAA have the smallest aperture area, very good bandwidth performance, adequate beamsteering capabilities, as well as very good realized gain over the desired frequency bands. Owing to their smaller form factor along with comparable performance metrics, the proposed structures will facilitate easier and better integration with other mm-wave circuits and devices. The proposed on-package SSCAA and DSCAA can easily be accommodated on the different edges of the phones in a multiple-input-multiple-output (MIMO) antenna configuration for covering different directions and support the increase in the throughput of the 5G wireless standards.

IV. CONCLUSION

In this work, two slot-based connected antenna array solutions are proposed for 5G mm-wave applications. The on-package SSCAA and DSCAA are designed in multilayer stack-up having four metal and three dielectric layers. Stripline-based feed lines are used for exciting the slots and BR is used to reflect the backward radiation from the slots in the upward directions. Through vias are used for passing the signals from the bottommost layer and for ensuring the ground connections. Microstrip and GCPW-based branched-out feed lines are used in the bottommost layer of both the structures. The on-package SSCAA and DSCAA have 3.18 GHz and 5 GHz of measured bandwidth in the desired frequency range, respectively. This is consistent with the literature, confirming that the 2D periodic arrays (planar array/DSCAA) of the CAA provide wider bandwidth than the 1D (linear array/SSCAA) counterparts. On-package SSCAA and DSCAA have a realized gain of 9.89 dBi and 12.5 dBi and efficiencies of 89% and 78% , respectively. The beams from the on-package SSCAA and the DSCAA are steered with an in-house built beamformer. Beamsteering up to $\pm 35^0$ is demonstrated. The proposed SSCAA and the DSCAA have radiator sizes of 1.63λ x 0.17λ x 0.1λ (17.5 mm x 1.9 mm x 1.077 mm) and 1.61λ x 0.48λ x 0.1λ (17.3 mm x 5.2 mm x 1.077 mm), respectively (λ centered at 28 GHz). The proposed prototypes have been compared with the state of the art solutions in terms of several performance criteria. The comparative demonstrations show that the proposed prototypes have very good bandwidth and realized gain with the smallest form factor. It is expected that the proposed on-package SSCAA and DSCAA will be a viable candidate for the 5G mm-wave applications.

This work is licensed under a Creative Commons Attribution-NonCommercial-NoDerivatives 4.0 License. For more information, see https://creativecommons.org/licenses/by-nc-nd/4.0/

This article has been accepted for publication in IEEE Open Journal of Antennas and Propagation. This is the author's version which has not been fully edited and content may change prior to final publication. Citation information: DOI 10.1109/OJAP.2024.3358373

TABLE 5. Comparison table with the literature for the AiP concepts at mm-wave.

Ref.	Frequency Bands (GHz)	BW (GHz)	Max. Realized Gain (dB)	Radiator Size	Antenna Type ans No. of Elements	beamsteering Capability
[7,11-16]	26.5–29.5 GHz (n257); 27.5–28.35 GHz (n261) ; 37–40 GHz (n260)	0.8	20 dB (antenna-5 dB, array-6 dB, beamforming-6 dB, pol-3 dB)	19.03 mm x 4.81 mm	1×4 dipole, 1×4 patch, 2×2 patch and 2×4 patch	Yes (±45°)
[9]	27.21–28.72 GHz; 36.96–40.17 GHz	1.51; 3.57	10.06 @ 28 10.63 dBi @39	19.2 mm × 4.2 mm × 0.84 mm	1x4 patch antenna array	Yes
[10]	28 GHz	4.3	10.8 dBi	30 mm x 16 mm x 992 µm	1x4 patch antenna array	Not reported
[17]	23–30.5 GHz	7.5	9.76 dBi	26 mm × 5 mm × 1.524 mm	1x4 patch antenna array, 2x3 parasitic square array	Yes (±30°)
[18]	28 GHz; 39 GHz	3	11.6 dBi Broadside; 10 dBi endfire	5.8 mm × 19 mm × 1.122 mm	patch and dipole array	Not reported
[19]	26.5—29.5 GHz	3	17.37 dBi	37.2 mm x 37.2 mm x 1.2 mm.	4 × 4 patch array; dual-polarized	Yes (±30°)
[20]	25.4 -–31.6 GHz	6.2	10.2 dBi	17.8 mm x 2 mm	SCAA (4x1) on phone rim	Yes (±30°)
[23]	27.03 –29.07 GHz	2	10.2 dBi	18.2 mm x 4.3 mm x 1.1 mm	SCAA (4x1)	Yes (±38°)
This work-SSCAA	25.87 –29.05 GHz	3.18	10.7 dBi	17.5 mm x 1.9 mm x 1.1 mm	SCAA (4x1)	Yes (±35°)
This work-DSCAA	27.7 –32.7 GHz	5	12.7 dBi	17.3 mm x 5.2 mm x 1.1 mm	SCAA (4x2)	Yes (±35°)

ACKNOWLEDGEMENTS

The authors would like to thank the Fonds de recherche du Québec Nature et Technologies (FRQNT) for the doctoral research scholarship provided to support this work. This work was also partially funded by NSERC project number RGPIN-2019-05298.

REFERENCES

[1] X. Xia et al., "Millimeter-Wave Phased Array Antenna Integrated With the Industry Design in 5G/B5G Smartphones," in IEEE Transactions on Antennas and Propagation, vol. 71, no. 2, pp. 1883-1888, Feb. 2023, doi: 10.1109/TAP.2023.3234173.

[2] D. Liu, Y. Zhang, *Antenna-in-Package Technology and Applications*, Wiley, 2020.DOI:10.1002/9781119556671

[3] D. Liu, B. Gaucher, U. Pfeiffer and J. Grzyb, *Advanced Millimeter-Wave Technologies: Antennas Packaging and Circuits*, Hoboken, NJ, USA:Wiley, 2009.

[4] Y. Zhang and J. Mao, "An Overview of the Development of Antenna-in-Package Technology for Highly Integrated Wireless Devices," in Proceedings of the IEEE, vol. 107, no. 11, pp. 2265-2280, Nov. 2019, doi: 10.1109/JPROC.2019.293326

[5] Y. P. Zhang and D. Liu, "Antenna-on-Chip and Antenna-in-Package Solutions to Highly Integrated Millimeter-Wave Devices for Wireless Communications," in IEEE Transactions on Antennas and Propagation, vol. 57, no. 10, pp. 2830-2841, Oct. 2009, doi: 10.1109/TAP.2009.2029295.

[6] D. Liu, X. Gu, C. W. Baks and A. Valdes-Garcia, "Antenna-in-Package Design Considerations for Ka-Band 5G Communication Applications," in IEEE Transactions on Antennas and Propagation, vol. 65, no. 12, pp. 6372-6379, Dec. 2017, doi: 10.1109/TAP.2017.2722873.

[7] A. O. Watanabe, M. Ali, S. Y. B. Sayeed, R. R. Tummala and M. R. Pulugurtha, "A Review of 5G Front-End Systems Package Integration," in IEEE Transactions on Components, Packaging and Manufacturing Technology, vol. 11, no. 1, pp. 118-133, Jan. 2021, doi: 10.1109/TCPMT.2020.3041412

[8] W. Hong, K. -H. Baek and S. Ko, "Millimeter-Wave 5G Antennas for Smartphones: Overview and Experimental Demonstration," in IEEE Transactions on Antennas and Propagation, vol. 65, no. 12, pp. 6250-6261, Dec. 2017, doi: 10.1109/TAP.2017.2740963.

[9] H. -C. Huang, R. Ma, X. Jian, Y. Wang and Z. Zhu, "A Miniaturized Band-Switching Multiband Dual-Polarized 5G mm-Wave Antenna-in-Package (AiP) Array for Cellular Phones," 2019 International Symposium on Antennas and Propagation (ISAP), Xi'an, China, 2019, pp. 1-3

[10] Y. -W. Lu, B. -S. Fang, H. -H. Mi and K. -T. Chen, "Mm-Wave Antenna in Package (AiP) Design Applied to 5th Generation (5G) Cellular User Equipment Using Unbalanced Substrate," 2018 IEEE 68th Electronic Components and Technology Conference (ECTC), San Diego, CA, USA, 2018, pp. 208-213, doi: 10.1109/ECTC.2018.00040.

[11] J. D. Dunworth et al., "A 28GHz Bulk-CMOS dual-polarization phased-array transceiver with 24 channels for 5G user and base station equipment," 2018 IEEE International Solid - State Circuits Conference - (ISSCC), San Francisco, CA, USA, 2018, pp. 70-72, doi: 10.1109/ISSCC.2018.8310188.

This work is licensed under a Creative Commons Attribution-NonCommercial-NoDerivatives 4.0 License. For more information, see https://creativecommons.org/licenses/by-nc-nd/4.0/

This article has been accepted for publication in IEEE Open Journal of Antennas and Propagation. This is the author's version which has not been fully edited and content may change prior to final publication. Citation information: DOI 10.1109/OJAP.2024.3358373

[12] Microwave Journal, "First 5g mmwave antenna module for smartphones". [Online]. Available: https://www.microwavejournal.com/articles/31448-first-5g-mmwave-antenna-module-for-smartphones.
[13] Y. Zhang, "Antenna-in-Package Technology: Its Early Development [Historical Corner]," in IEEE Antennas and Propagation Magazine, vol. 61, no. 3, pp. 111-118, June 2019, doi: 10.1109/MAP.2019.2907916.
[14] https://www.qualcomm.com/news/releases/2018/07/qualcomm-delivers-breakthrough-5g-nr-mmwave-and-sub-6-ghz-rf-modules-mobile
[15] https://www.qualcomm.com/news/releases/2019/02/qualcomm-announces-second-generation-5g-rf-front-end-solutions-sleeker-more
[16] https://www.qualcomm.com/news/releases/2020/02/qualcomm-introduces-third-generation-5g-modem-rf-system-enhance-5g
[17] C. -Y. -D. Sim, J. -J. Lo and Z. N. Chen, "Design of a Broadband Millimeter-Wave Array Antenna for 5G Applications," in IEEE Antennas and Wireless Propagation Letters, vol. 22, no. 5, pp. 1030-1034, May 2023, doi: 10.1109/LAWP.2022.3231358
[18] J. Seo et al., "Miniaturized Dual-Band Broadside/Endfire Antenna-in-Package for 5G Smartphone," in IEEE Transactions on Antennas and Propagation, vol. 69, no. 12, pp. 8100-8114, Dec. 2021, doi: 10.1109/TAP.2021.3088230
[19] W. Kim, J. Bang and J. Choi, "A Cost-Effective Antenna-in-Package Design With a 4 × 4 Dual-Polarized High Isolation Patch Array for 5G mmWave Applications," in IEEE Access, vol. 9, pp. 163882-163892, 2021, doi: 10.1109/ACCESS.2021.3133284.
[20] R. S. Malfajani, F. B. Ashraf and M. S. Sharawi, "A 5G Enabled Shared-Aperture, Dual-Band, in-Rim Antenna System for Wireless Handsets," in IEEE Open Journal of Antennas and Propagation, vol. 3, pp. 1013-1024, 2022, doi: 10.1109/OJAP.2022.3201627.
[21] A. Neto and J. J. Lee, "Infinite Bandwidth Long slot array antenna," *IEEE Antennas Wireless Propag. Lett*, vol.4, pp. 75-78, 2005.
[22] D. Cavallo, "Connected array antennas: analysis and design," Doctoral dissertation, TU Eindhoven, 2011.
[23] A. Neto, D. Cavallo, G. Gerini and G. Toso, "Scanning Performances of Wideband Connected Arrays in the Presence of a Backing Reflector," *IEEE Trans. Antennas Propag.*, vol.57, no.10, pp. 3092-3102, Oct. 2009.
[24] M. Rasheduzzaman Al-Amin and M. S. Sharawi, "on-package Connected Array with beam-steering Capabilities at Millimeter-Waves," 2021 15th European Conference on Antennas and Propagation (EuCAP), Dusseldorf, Germany, 2021, pp. 1-4, doi: 10.23919/EuCAP51087.2021.9410946.
[25] D. M. Pozar, "Microwave Engineering", Hoboken, NJ: Wiley, 2012.
[26] Y. Tao and F. Scharf, "Revisiting the Effect of Nickel Characteristics on High-Speed Interconnect Performance," in IEEE Transactions on Microwave Theory and Techniques, vol. 64, no. 8, pp. 2447-2453, Aug. 2016, doi: 10.1109/TMTT.2016.2586943.



MD RASHEDUZZAMAN AL-AMIN (Graduate Student Member, IEEE) received the B.Sc. and M.Sc. degrees in Electrical and Electronic Engineering from the Islamic University of Technology, Gazipur, Bangladesh, in 2011 and 2016, respectively. Currently, he is pursuing the Ph.D. degree in the Electrical Engineering Department at the University of Montréal (Polytechnique Montréal), Montreal, QC, Canada. His research interests include microwave and millimeter-wave (mm-wave) antenna design, phased array, connected antenna array, and antenna-in-package (AiP). Mr Al-Amin was a recipient of the 2021 IEEE Antennas and Propagation Society (AP-S) Doctoral Research Grant. He received the Fonds de Recherche du Québec Nature et Technologies (FRQNT) Doctoral Scholarship in 2020.



REZA SHAMSAEE MALFAJANI (Graduate Student Member, IEEE) received the B.S. degree in electrical engineering from the University of Tehran, Tehran, Iran, in 2009 and the M.S. degree in electrical engineering from Tarbiat Modares University, Tehran, in 2012. He is currently pursuing a Ph.D. degree with the Polytechnique Montréal, Montreal, QC, Canada. He is also a member of the Poly-Grames Research Center, Polytechnique Montréal. His research focuses on the periodic structures, antennas and RF, mm-wave, and Terahertz designs. He received the Merit Scholarship Program for Foreign Students (PBEEE) in 2023, the Jocelyne and Jean C. Monty Doctoral Research Excellence Scholarship in 2022, and Food Agility CRC Scholarship in 2021.



Elham Baladi (Member, IEEE) received the B.Sc. degree in electrical engineering – communications from the Iran University of Science and Technology, Tehran, Iran, in 2013, and the Ph.D. degree in electromagnetics and microwaves from the University of Alberta, Edmonton, AB, Canada, in January 2019. She developed a novel class of resonant metasurfaces during her Ph.D. degree and investigated their applications for shielding, imaging, and selective transmission. Dr. Baladi was a postdoctoral fellow with the University of Toronto, Toronto, ON, Canada, from February 2019 to February 2021, where she conducted research on the modeling and development of reconfigurable antenna arrays for space applications. She was an Antenna and RF Filter Design Engineer with Syntronic Research and Development Canada, Ottawa, ON, Canada, from February 2021 to August 2022, where she worked on the development of RF cavity filters, duplexers, and multi-band antennas for 5G, IoT, and wireless communication systems. Dr. Baladi joined the Electrical Engineering department of Polytechnique Montreal, Montreal, QC, Canada, as an Assistant Professor in September 2022. Her research interests include the development of novel multi-band multi-beam antenna arrays, metasurfaces, reconfigurable intelligent surfaces, microwave sensors, and radar imaging techniques. Dr. Baladi was the recipient of the University of Alberta Doctoral Recruitment scholarship, the Alberta Innovates Technology Futures scholarship, the IEEE AP-S Doctoral Research Award, and two honorable mention awards in the student-paper competitions of the 2016 and 2017 IEEE AP-S Symposia. She has been a lecturer at York University (Winter 2020) and the University of Alberta (Winter 2017) and serves as a Reviewer for multiple IEEE and OSA journals. She also currently serves as the chair of the IEEE Antenna and Propagation Section and Vice Chair of IEEE Women in Engineering in Montreal.



MOHAMMAD S. SHARAWI (Fellow, IEEE) is currently a Lead Engineer at Blue Origin LLC working on research and development projects for space communication systems. He was a Full tenured Professor of electrical engineering with Polytechnique Montréal, Montreal, QC, Canada between 2019-2023. Dr. Sharawi was with King Fahd University of Petroleum and Minerals, Dhahran, Saudi Arabia, from 2009 to 2018, where he founded and directed the Antennas and Microwave Structure Design Laboratory (AMSDL). He was a Visiting Professor with the Intelligent Radio Laboratory (iRadio), Department of Electrical Engineering, University of Calgary, Calgary, AB, Canada, in summer, fall 2014. He was a Visiting Research Professor with Oakland University, Rochester, MI, USA , during 2023 and in 2013. Dr. Sharawi has more than 400 papers published in refereed journals and international conferences, 11 book chapters (two of which in the Antenna Handbook, fifth edition, McGraw Hill, 2018), one single authored book titled Printed MIMO Antenna Engineering (Artech House, 2014), the Lead Author of the book Design and Applications of Active Integrated Antennas (Artech House, 2018), and a co-author of the upcoming book MIMO Antenna Systems for 5G and Beyond (IEEE-Wiley, 2024). He has 28 issued/granted and ten pending patents in the US Patent Office. His research interests

This work is licensed under a Creative Commons Attribution-NonCommercial-NoDerivatives 4.0 License. For more information, see https://creativecommons.org/licenses/by-nc-nd/4.0/

This article has been accepted for publication in IEEE Open Journal of Antennas and Propagation. This is the author's version which has not been fully edited and content may change prior to final publication. Citation information: DOI 10.1109/OJAP.2024.3358373

include multiband printed multiple-input–multiple-output (MIMO) antenna systems, reconfigurable and active integrated antennas, millimeter-wave antennas, integrated 4G/5G and beyond 5G antenna systems, shared aperture and encapsulated antennas, microwave sensors, applied electromagnetics, sub-THz structures, and computational methods. He received his MSc. and PhD. degrees from Oakland University, Michigan, USA, in 2002 and 2006, respectively.

Dr. Sharawi was a recipient of the Abdul Hameed Shoman Foundation Award for Arab Researchers for the category of wireless systems in 2020 in addition to various best IEEE conference paper awards. He has served on the Technical and Organizational Program Committees as well as organized several special sessions on MIMO antenna systems and their applications in 4G and 5G wireless systems in several international conferences, such as European Conference on Antennas and Propagation (EuCAP), Antennas and Propagation Society (APS), International Microwave Workshop Series on 5G Hardware and System Technologies (IMWS-5G), Asia-Pacific Conference on Antennas and Propagation (APCAP), International Workshop on Antenna Technology (iWAT), among many others for many years. He has served as the IEEE APS Chair for the Montreal Section (2020–2023) and an Active Member for the IEEE Member Benefits Committee leading the initiative of the APS Student Travel Grant. He is also the Regional Delegate of the EuRAAP in North America until Dec. 2023. He was an Associate Editor of IEEE Antennas and Wireless Propagation Letters from 2019 to 2023. He was the Specialty Chief Editor of the newly launched Frontiers in Communications and Networks for the System and Test-Bed Design Section from 2020 to 2022. He is serving as an Associate Editor for the IEEE Open Journal of Antennas and Propagation and IET Microwaves, Antennas and Propagation (Wiley), and an Area Editor (antennas and microwave devices and systems) for Microwave and Optical Technology Letters (Wiley). He is a Distinguished Lecturer (DL) for APS for the period 2023–2025, a Fellow of the IEEE and IET.

This work is licensed under a Creative Commons Attribution-NonCommercial-NoDerivatives 4.0 License. For more information, see https://creativecommons.org/licenses/by-nc-nd/4.0/